A Precise Measurement of the Nuclear Dependence of Structure Functions in Light Nuclei.

J. Arrington (spokesperson), D. F. Geesaman, K. Hafidi, R. Holt
H. E. Jackson, D. H. Potterveld, P. E. Reimer, B. Zeidman, X. Zheng
Argonne National Laboratory, Argonne, IL

F. Dohrmann
Forschungszentrum Rossendorf, Dresden, Germany

O. K. Baker, M. E. Christy, C. E. Keppel
Hampton University, Hampton, VA

I. Niculescu
James Madison University, Harrisonburg, VA

R. Ent, H. Fenker, D. Gaskell, A. F. Lung, D. J. Mack,
D. G. Meekins, J. Roche, G. Smith, G. Warren
Jefferson Laboratory, Newport News, VA

D. Crabb, D. Day, P. McKee, O. Rondon, F. Wesselmann, H. Zhu
University of Virginia, Charlottesville, VA

R. Asaturyan, H. Mkrtchyan, V. Tadevosyan
Yerevan Physics Institute, Armenia

April 25, 2003

Abstract

We propose to measure inclusive electron scattering from ^{1}H, ^{2}H, ^{3}He, and ^{4}He over a broad range of x $(0.3 < x < 1.0)$ up to $Q^2 \approx 8.0$ GeV^2. For ^{4}He, the measurement will be of significantly better precision than previous data, while for ^{3}He there is almost no data on the unpolarized structure functions in the valence region. With this data, we can make a precision measurement of the EMC effect in few-body nuclei. While the EMC effect has been measured on ^{4}He, the uncertainties are large enough that the data cannot distinguish between different models for the A-dependence in light nuclei. We will improve the precision on ^{4}He by a factor of two over existing measurements, as well as making the first measurement of the EMC effect on ^{3}He for $x > 0.5$. This will test the A-dependence of various models of the EMC effect, as well as allowing comparison to 'exact' calculations of the EMC effect in few-body nuclei. These light nuclei may be especially important in understanding the

EMC effect because while heavy nuclei all show the same shape (x-dependence) to the EMC effect, several models predict a significantly different shape in few-body nuclei. Thus, these data will be able to distinguish between models based on both their A-dependence and their x-dependence. A better understanding of the EMC effect, especially in light nuclei, will also provide guidance for calculations of nuclear effects in deuterium. This precise set of data on ^{1}H, ^{2}H, ^{3}He and ^{4}He can be used to test models of nuclear effects in few-body nuclei. This will allow for an improved understanding of the systematic uncertainties in the procedures used to extract the neutron structure function from measurements on nuclear targets.

1 INTRODUCTION

Lepton scattering is an almost ideal probe for studying the quark substructure of nucleons and nuclei. The interaction of the electromagnetic probe with the quarks is well understood theoretically, and the relatively weak coupling allows for a clean separation of the scattering mechanism from the target structure. The weak coupling is especially important in probing nuclei because the scattering is not strongly modified by additional interactions with the target, and because it means that interior of the nucleus is not shielded by the outer nucleons. Leptonic probes have been used to make precise measurements of the polarized and unpolarized structure functions of the proton. The parton model predicts that at large momentum transfer, q, and energy transfer, ν, the structure functions depend only on Bjorken-x [$x = (q^2 - \nu^2)/2m_p\nu = Q^2/2m_p\nu$]. The structure functions measured in this limit can be directly related to the quark distributions of the target, allowing one to extract polarized and unpolarized quark distributions within the nucleon or nucleus.

In addition to providing nuclear structure functions, this is also a primary method of obtaining information on the neutron structure function. Direct scattering measurements from neutrons are not feasible since neutron targets of adequate density are not available. Therefore, most of the information on (unpolarized) neutron structure comes from comparisons of the proton and deuteron structure functions. Extraction of the neutron structure function depends not only on precise measurements on the proton and deuteron, but also on the understanding of nuclear effects in the deuteron. The European Muon Collaboration (EMC) discovered [1] that the nuclear structure function is significantly different from the sum of nucleon structure functions, showing that these nuclear effects are non-trivial. Measurements of the EMC effect in light nuclei will provide guidance for modeling of nuclear effects in the deuteron, which is necessary to extract the neutron structure function. In addition, measurements of the EMC effect in ^{3}He and ^{4}He will allow direct comparison to exact, few-body calculations of the EMC effect, which cannot be performed for heavier nuclei. This will help isolate the microscopic origin of the EMC effect, and thus better understand it for both light and heavy nuclei.

2 MOTIVATION

2.1 The EMC Effect

Extensive structure function measurements have been made on nuclear targets. The European Muon Collaboration used muon scattering to measure nuclear structure functions [1]. The initial goal of using nuclear targets was to increase luminosity, but the structure functions measured in scattering from iron and deuterium differed substantially. When they compared the cross section per nucleon, they saw an enhancement in iron below $x \approx 0.3$ and a suppression at larger values of x. Figure 1 shows the ratio $\sigma_{Fe}/\sigma_{^2H}$ as a function of x for measurements by the EMC collaboration [1], the BCDMS collaboration [2], and SLAC experiment E139 [3]. This nuclear dependence, termed the EMC effect, has since been measured for several targets and mapped out over a large kinematical range. Following these measurements, several theoretical models have been used in an attempt to explain the effect. While it is now possible to identify some of the ingredients necessary to explain the nuclear dependence of the structure function, other components are still unknown, and there exist competing models based on significantly different pictures of the effect. An overview of measurements and models of the EMC effect can be found in ref. [4].

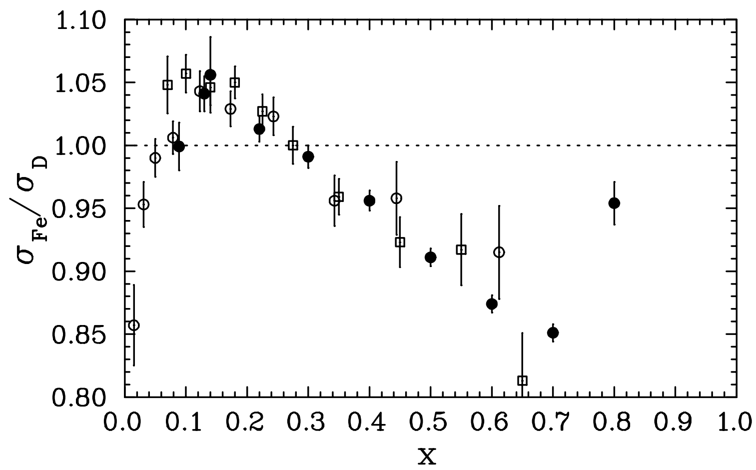

Figure 1: $(\sigma_{Fe}/\sigma_{^2H})$ ratios as a function of x from EMC (hollow circles), SLAC (solid circles), and BCDMS (squares). The data have been averaged over Q^2 and corrected for neutron excess.

Several approaches have been used to try to explain the observed nuclear dependence of the cross section. If one expresses the nuclear structure function as a convolution of the proton and neutron structure functions, the modification can be generated in one of two ways: either the nucleon structure is modified when in the nuclear medium, or the nuclear structure function is modified in the convolution due to multi-nucleon effects (binding, exchange pions, N-N correlations, etc...). Models using both approaches have attempted to explain the EMC effect. While many of these models have had some success, they typically reproduce only part of the observed enhancement or suppression, explain a limited x range, or are in conflict with other measurements. Calculations which simply include the momentum distribution of the nucleons predicted that the effect would be below the few percent level for $x \leq 0.6$ [5] (*i.e.* away from the quasielastic peak), which is significantly smaller than is observed. Models which also include the removal energy of the nucleon (Akulinichev *et al.* [6], Ciofi degli Atti and Liuti [7]) have been able to reproduce certain aspects of the data, but have failed to reproduce either the magnitude or the low x behavior of the effect. The EMC effect has also been modeled in terms of an enhancement of the pion field within a nucleus. The pion exchange piece of the nucleon-nucleon interaction leads to a modification of the virtual pion cloud in the nucleus, producing a shifting of strength in x. However, this requires a pion excess that is too large to be consistent with a Drell-Yan measurement of the pion modification in nuclei [8]. Recently, Smith and Miller [9] have concluded that the binding of the nucleons alone cannot explain the EMC effect, and that explicit mesonic components appear to be insufficient due to the limits set by the Drell-Yan measurements. They conclude that it is likely that a complete explanation is not possible within a purely hadronic model, and that some modification to nucleon structure is needed.

The nuclear dependence has also been modeled in terms of a change in the confinement radius of a nucleon bound in a nucleus. This leads to a 'swollen' nucleon, which will have a softer valence quark distribution. While this picture can reproduce the magnitude and x-dependence of the EMC effect fairly well, it requires a significant increase in the size of the nucleon ($\sim$15% in iron). This would have observable effects in other experiments, and a swelling of this size appears to be ruled out [10, 11, 12]. Ultimately, the EMC effect may be fully described by one of the mechanisms currently being examined, by some new approach, or by some combination of these models. In order to determine which model best describes reality, we need to measure the EMC effect over as broad a range in x, Q^2, and A as possible to separate models by their specific predictions.

The most complete measurements of the EMC effect come from SLAC experiment E139 [3]. They measured ratios to deuterium for ^{4}He, ^{9}Be, ^{12}C, ^{27}Al, ^{40}Ca, ^{56}Fe, ^{108}Ag, and ^{197}Au targets for three Q^2 bins (Q^2=2 and 5 GeV^2 for $x < 0.3$; Q^2=2, 5, and 10 for $0.3 \leq x \leq 0.5$; Q^2=5 and 10 for $x > 0.5$). In addition to measuring the x-dependence, E139 examined the Q^2-dependence and A-dependence of the effect. They found no significant Q^2-dependence in the measured cross section ratios. The ratio does have a strong target dependence which, at fixed x, can be well described as a function of mass number ($\sigma_A/\sigma_{^2H} = C(x)A^{\alpha(x)}$, where their fit yields $C(x) \approx 1$) or as a function of the average nuclear density, ρ ($\sigma_A/\sigma_{^2H} = D(x)[1 + \beta(x)\rho(A)]$, with $\beta(x) \approx 1$). For the SLAC analysis (and in this proposal) ρ is taken to be the nuclear density (nucleons/fm^3) determined assuming a uniform sphere with a radius equal to the RMS electron scattering charge radius [3, 13]. The measured target dependence of the EMC effect is shown in figure

2, along with fits to a $\log(A)$ dependence and a density dependence [3]. While the ^{4}He/D ratio provides the greatest sensitivity for determining if the nuclear dependence is best described as an A-dependence or a ρ-dependence, the uncertainty in the present data is large and the ratio is consistent with both parameterizations. It is also possible that neither of these descriptions is adequate to describe the EMC effect in very light nuclei. A better measurement for few-body nuclei is necessary if we want to extend models of the EMC effect to the deuteron.

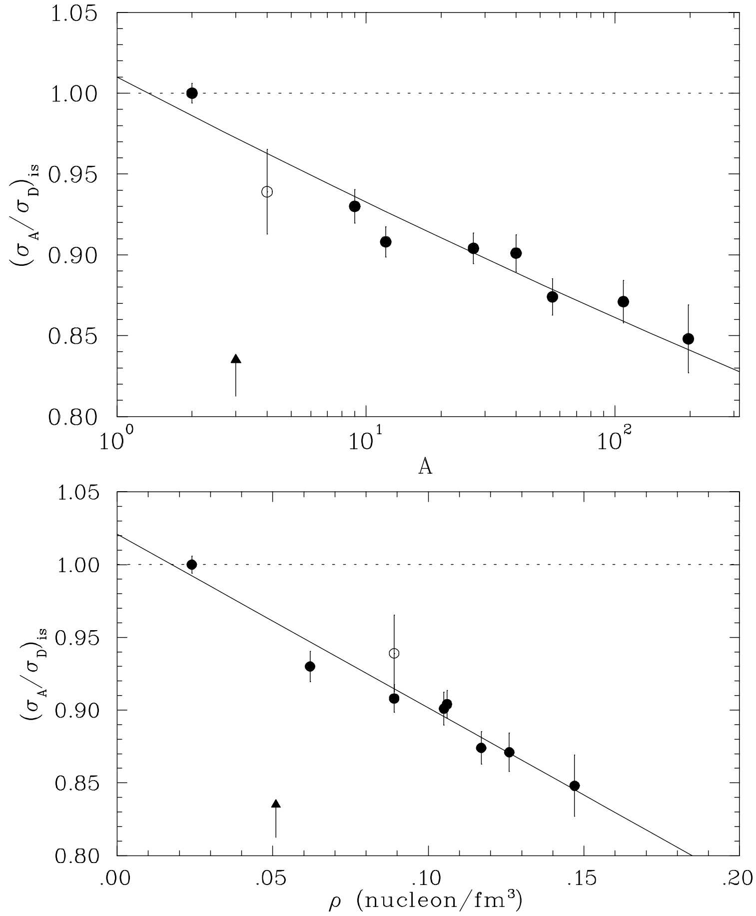

Figure 2: $(\sigma_A/\sigma_{^2H})$ ratios at x=0.6 from E139 plotted as a function of mass number and nuclear density. The data is averaged over all Q^2 and corrected for neutron excess. Errors include statistical uncertainties, point-to-point and target-to-target systematic uncertainties. The hollow point is the data for ^{4}He, and the arrow indicates the value of A (ρ) for ^{3}He.

At Jefferson Lab, we can improve our understanding of nuclear effects in light nuclei by measuring the EMC effect in ^{3}He and ^{4}He. Table 1 shows A, ρ, and the ratio of ρ to $\log(A)$ (taken relative to ^{27}Al) for selected nuclear targets. For the carbon and the heavier targets

Nucleus	A	$\rho(\mathrm{fm}^{-3})$	$[\rho/\log(A)]/[\rho/\log(A)]_{Al}$
^{2}H	2	0.024	1.08
^{3}He	3	0.051	1.44
^{4}He	4	0.089	2.00
^{9}Be	9	0.062	0.88
^{12}C	12	0.089	1.11
^{27}Al	27	0.106	1.00
^{40}Ca	40	0.105	0.87
^{56}Fe	56	0.117	0.90
^{108}Ag	108	0.126	0.84
^{197}Au	197	0.147	0.87

Table 1: Mass number and nuclear density for ^{3}He and the nuclei used in E139. The density is determined assuming a uniform sphere with a radius equal to the RMS charge radius determined from electron scattering. For ^{3}He, the proton radius is significantly different than the neutron radius. Using a calculated value for the neutron radius, or assuming that the ^{3}He neutron radius is equal to the ^{3}H proton radius, the value extracted for the nuclear density becomes somewhat higher (0.053-0.055)

the difference between a linear density dependence and an A^{α} dependence is relatively small ($\rho/\log(A)$ varies at the 10-15% level). However, ^{3}He and ^{4}He have a significantly different dependence of density on mass number. ^{4}He is the lightest nucleus for which the EMC effect has been measured, and while it can in principle distinguish a logarithmic (A) dependence from a linear density dependence, the current measurement is not sufficient to distinguish between the two models. The proposed measurement will use a significantly denser ^{4}He target, thus reducing the uncertainty in the target thickness which was the dominant systematic uncertainty in the ratio for E139. In addition, the denser target, combined with the high beam current and large acceptance spectrometers will allow a significant improvement in the statistical precision of the measurement. We expect to reduce the total uncertainty in $\sigma_{^4He}/\sigma_{^2H}$ by nearly a factor of two. ^{3}He is lower in both mass number and nuclear density than any nucleus for which the EMC effect has been measured, so the addition of data on ^{3}He will be important in parameterizing the nuclear dependence of the EMC effect in light nuclei, and will provide the first measurement of the EMC effect in ^{3}He for $x > 0.5$.

For heavy nuclei ($A \geq 9$), the magnitude of the EMC effect (the deviation from unity of $\sigma_A/\sigma_{^2H}$) varies with A, but the x-dependence is nearly constant. Most parameterizations of the EMC effect assume that the shape of the effect is constant or depends very weakly on A for all nuclei, except at very large values of x ($x > 0.8$), where $\sigma_A/\sigma_{^2H}$ is dominated by the Fermi smearing. The observed x-dependence in ^{4}He is consistent with the heavier nuclei, but the uncertainties in the measurement are much larger, and it is not possible to rule out a significant difference in shape. Several more recent works [14, 15, 16] have suggested that the EMC effect for $A \leq 4$ will differ from heavy nuclei not only in the size of the effect, but also in the shape. They predict differences in the point of maximum suppression and the point where the EMC ratio crosses unity (at very large x). Figure 3 shows the existing data for ^{4}He, along with three different models for the x-dependence. The dashed line is the fit to heavy nuclei, the dotted line is the calculations of Ref. [14], and the solid line is the calculation of Ref. [15].

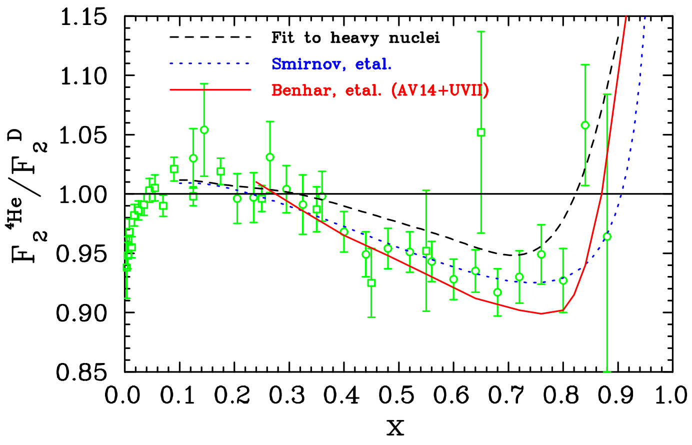

Figure 3: $(\sigma_{^4He}/\sigma_{^2H})$ ratios as a function of x from EMC (hollow circles), compared to the fit to heavy nuclei (scaled to A=4) and two calculations [14, 15].

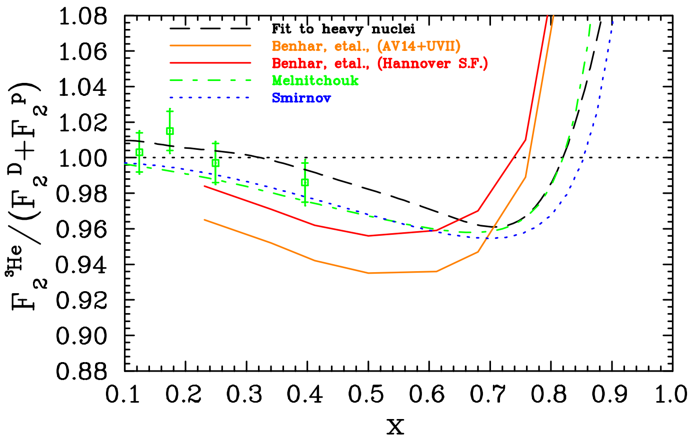

Figure 4: $(\sigma_{^3He}/\sigma_{^2H})$ ratios as a function of x from HERMES (hollow circles). The dashed black line is the fit to heavy nuclei, scaled to ^{3}He, while the solid red and orange lines are the calculations of Benhar *et al.* [15], the dotted blue line is the calculation of Smirnov *et al.* [14], and the dot-dashed green line is the calculation of Afnan *et al.* [16].

We propose to measure the EMC ratio $(\sigma_A/\sigma_{^2H})$ for ^{3}He and ^{4}He, covering $x \gtrsim 0.3$.

We will improve the uncertainty for ^{4}He, which will significantly improve our ability to distinguish an A-dependence from a ρ-dependence for the EMC effect. We will also make the first measurement of the EMC effect for $A = 3$ and large x, which will increase our range in A (and in ρ) compared to the previous measurements. The HERMES collaboration has measured $\sigma_A/\sigma_{^2H}$ [17] for ^{3}He, but the bulk of the data is at extremely small x values (in the shadowing region). They have measurements at larger x values, but the uncertainties are large for $x > 0.5$, and while the shape is consistent with the EMC effect observed in other nuclei, the ratio is also consistent with unity (no nuclear effects). In addition to improving the measurements of the EMC effect in light nuclei, the proposed measurement will extend the kinematics to somewhat lower Q^2 than the previous measurements. While the SLAC measurements showed no indication of a Q^2 dependence, most of the measurements are above $Q^2 \approx 5$ GeV^2. Most of the data at lower Q^2 is for $x < 0.5$, where the deviation of the EMC ratio from unity is very small and therefore only a large relative change in this deviation would be observable in the data. The proposed measurement will investigate the Q^2 dependence down to $Q^2 \sim$ 1-2 GeV^2.

2.2 Neutron Structure Function

Measurements of nuclear structure functions are also important for the understanding of the structure of the neutron. As free neutron targets are not available and neutron beams are too low in energy or intensity, information on the neutron structure is generally taken from measurements on nuclear targets. Current data for the neutron structure function come from measurements on deuterium and hydrogen, using models of the nuclear effects to remove the proton contribution to the deuterium measurements [18, 19]. The ability to extract the neutron structure from measurements on deuterium depends on our knowledge of the proton structure function, the deuteron momentum distribution, and the procedure used to extract the neutron component. The extraction must include a model of nuclear effects beyond the nucleon momentum distribution, and this model must be tested in order to be confident that it adequately describes all of the necessary nuclear effects.

Measurements of the neutron structure function are needed to understand the quark structure of nucleons. The difference between the structure of the neutron and that of the proton is sensitive to the u-quark and d-quark distributions in the proton. In particular, the ratio of the neutron to proton structure function as x approaches unity is sensitive to the high-x u-quark and d-quark valence distributions. Several predictions exist for this ratio at $x = 1$. SU(6) spin-flavor symmetry predicts $u_v^p(x) = 2d_v^p(x)$, and $d_v^n(x) = 2u_v^n(x)$, where $u_v(d_v)$ is the up(down) valence distribution in the proton or neutron. This leads to a value of $F_2^n(x)/F_2^p(x) = 2/3$ for large values of x (*i.e.* where the valence quarks dominate). DIS measurements indicate that SU(6) symmetry is broken, and that the proton d-quark distribution is softer than the u-quark distribution. If u-quark dominance is assumed (*i.e.* only u-quarks contribute in the limit $x \approx 1$), the prediction is $F_2^n(x)/F_2^p(x) \to 1/4$ as $x \to 1$. Other assumptions lead to a prediction that the ratio of d/u at large x is non-zero.

Models by Farrar and Jackson [20], and Brodsky *et al.* [21] predict that $u/d \to 5$ as $x \to 1$, and thus $F_2^n/F_2^p \to 3/7$. The initial analysis of SLAC and EMC experiments [18, 22] indicated a value close to 1/4, but the extraction of the neutron structure function only included corrections for the momentum distribution in the deuteron and did not include binding effects. A later analysis [24], including binding effects, found a value closer to the 3/7 prediction. Figure 5 shows the extracted F_2^n/F_2^p ratio using both an on-shell prescription that only includes the momentum distribution and an off-shell prescription that includes binding. Clearly, the off-shell effects are very important, and additional data that can be used to check these models is needed to determine how accurately we can extract the neutron structure from measurements on the deuteron.

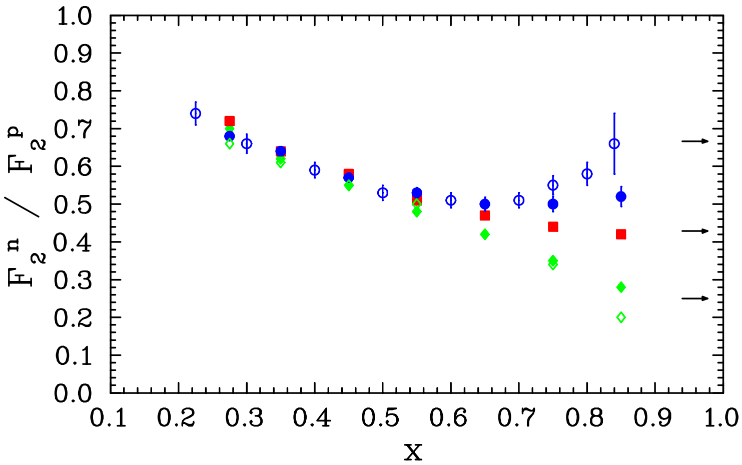

Figure 5: Ratio of F_2^n/F_2^p extracted from the SLAC measurements [3, 23] using on-shell prescriptions [24, 5](green diamonds), an off-shell prescription [24] (red squares), and models of the EMC effect scaled to deuterium [5, 10] (blue circles) to extract the neutron structure function. The arrows indicate the $x \to 1$ limits discussed in the text (1/4, 3/7, and 2/3).

We can test models of the nuclear effect by comparing their predictions for the EMC effect in light nuclei. However, we can also made different extractions of nucleon structure, using heavier nuclei, to test these models. For example, we can choose a model of the nuclear effects and use the ^{3}He and ^{2}H measurements to extract the proton structure function. This procedure depends on modeling the nuclear effects in both deuterium and ^{3}He. Since the nuclear effects are larger in this case, the model dependence will be greater than in the extraction of the neutron from ^{2}H and ^{1}H. If the proton structure as extracted from ^{3}He and ^{2}H is in good agreement with the direct measurements, this will help to quantify the uncertainties in the extraction of the neutron structure.

In recent years, several ideas have been suggested to measure neutron structure at large x in a model-independent fashion (or at least with significantly reduced model dependence) [25, 26]. This does not obviate the need for these measurements on light nuclei. While model-independent do not exist, this data will be useful in constraining the models used to extract the neutron structure from measurements in light nuclei. Once we have model-independent extractions of the neutron structure at large x, they will significantly improve our ability to measure the nuclear effects in light nuclei by removing the uncertainty arising from the lack of knowledge of the neutron structure functions.

3 KINEMATIC COVERAGE, SCALING, AND DUALITY

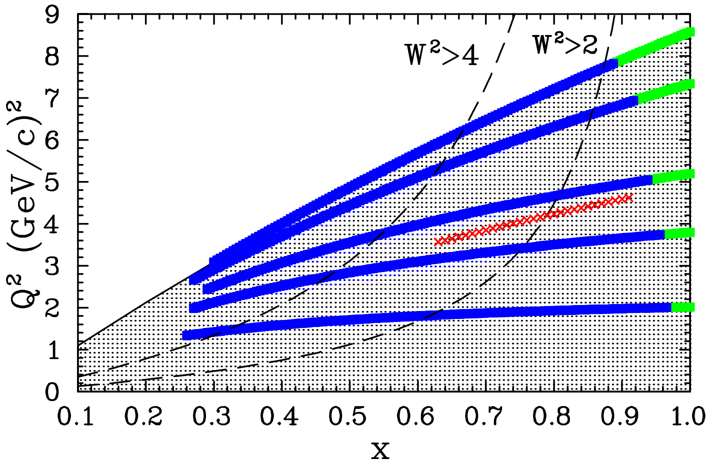

Figure 6: Overview of the proposed kinematics. The dark (blue) lines indicate the coverage for hydrogen (limited at high-x values by the rapidly falling cross section) and the light (green) lines indicate the additional coverage for the nuclear targets. The dashed lines correspond to W^2=2.0 and 4.0 GeV^2. The red crosses indicate the kinematics for the E89-008 data shown in Fig. 11

Figure 6 shows the proposed kinematic coverage at 6 GeV ($\theta \leq 60°$) as a function of x and Q^2. The data above $Q^2 = 4.0$ GeV^2 and at $W^2 > 4.0$ GeV^2 (to the left of the dashed line) are in the standardly defined DIS region. For $x < 0.65$, we will have DIS data for EMC ratios, neutron extraction, and tests of models of nuclear effects in deuterium and helium. In the DIS region, we see scaling of the structure function in x, but also in the Nachtmann variable, $\xi = 1/(1 + \sqrt{1 + 4m^2x^2/Q^2})$. For very large Q^2, $\xi \to x$, and so in the DIS limit the structure function will scale in ξ, and $F_2(\xi)$ will be related to the quark momentum distribution in the target, as is the case for x. However, the scaling violations at finite Q^2 are smaller when the data is examined in terms of ξ rather than x. This can be interpreted in terms of corrections to x for the effects of finite target mass, and it has also been shown that in the operator product expansion, ξ is the correct variable to use to disentangle the QCD scaling violations [27] from higher-twist effects.

While the data at higher x are below the typical cut for DIS scattering, we believe that the scaling of the structure function will continue. Inclusive measurements designed

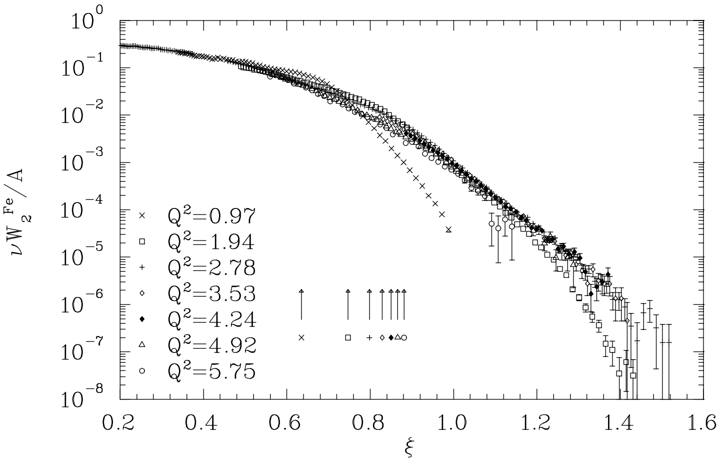

Figure 7: Structure function for iron as a function of ξ. The data are taken at fixed scattering angle, and the quoted Q^2 is the value for $x = 1$. The arrows indicate the value of ξ corresponding to the quasielastic peak for each setting.

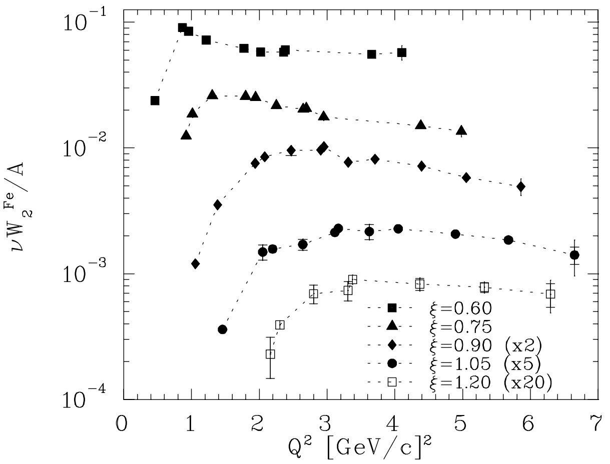

Figure 8: Structure function for iron at fixed ξ values as a function of Q^2. Inner errors are statistical, outer errors are statistical and systematic added in quadrature.

to probe $x > 1$ [28, 29] saw that scaling in scattering from nuclei occurred at kinematics far from the DIS region. Figure 7 shows the structure function for iron plotted against ξ. In iron, the smearing caused by the Fermi motion causes resonance structure and even the quasielastic (QE) peak disappear at high Q^2. Once the resonance structure has been washed out, we observe scaling at all ξ, both in the resonance region and even when the data is almost entirely dominated by quasielastic scattering. Figure 8 shows the structure function for iron as a function of Q^2 for several values of ξ. The structure function above Q^2=2-3 GeV^2 is constant to better than 10-20%. Scaling violations resulting from QCD evolution would be expected to cause variations of roughly 10% for large values of x. The largest remaining scaling violations occur at the top of the quasielastic peak (at the Q^2 yielding $x = 1$ at the given ξ value). Both the QCD scaling violations and the violations coming from the QE peak will be reduced at the lower values of x of the proposed measurements. They will also decrease as Q^2 increases and the quasielastic contribution becomes a smaller fraction of the total cross section.

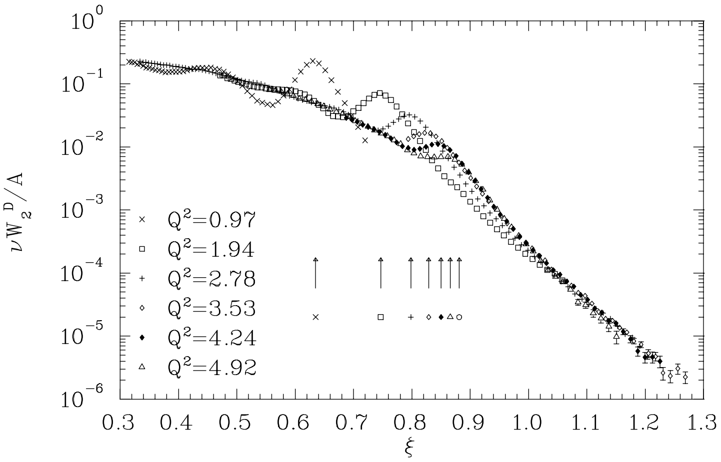

Figure 9: Structure function for deuterium as a function of ξ. The data are taken at fixed scattering angle, and the quoted Q^2 is the value for $x = 1$. The arrows indicate the value of ξ corresponding to the quasielastic peak for each setting.

Figure 9 shows the structure function for deuterium as a function of ξ. In this case, the quasielastic peak is clearly visible in the structure function, as is the resonance structure at lower Q^2, and the scaling that was observed in iron breaks down. As Q^2 increases the peaks move to higher ξ, but fall in strength in such a way as to roughly follow the curve in the scaling region. However, for $Q^2 \gtrsim 3$ GeV^2 the resonance structure is washed out and even the Δ resonance is no longer visible. Because deuterium has the lowest Fermi momentum, ξ-scaling should break down sooner (at higher W and Q^2) in deuterium than in any other nuclear target. Figure 10 shows the Q^2-dependence of the structure function for deuterium at fixed values of ξ from JLab experiment E89-008 [29] and SLAC measurements [30]. While the data covering the resonance region and DIS is sparse at large ξ, the data at moderate Q^2 values shows only the logarithmic QCD scaling violations down to $W^2 \approx 2$ GeV^2. The success of ξ-scaling in deuterium at extremely low values of W (above the QE peak) and relatively low momentum transfers leads us to believe that the very precise scaling observed in the DIS region should extend below $W^2 = 4$ GeV^2, especially for the larger Q^2 values of this measurement.

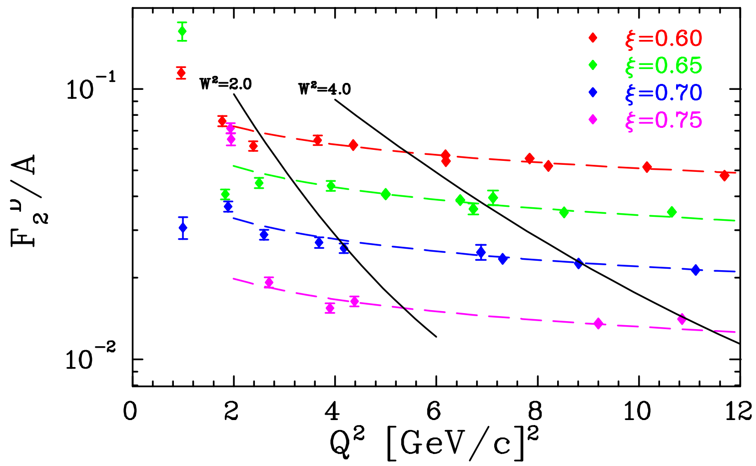

Figure 10: Structure function for deuterium as a function of Q^2 at fixed ξ values.

In the Bjorken limit, the parton model predicts that the structure function will scale, and that the scaling curve is directly related to the quark distributions. At large ν and Q^2, in the usual DIS region (W^2, $Q^2 > 4$ GeV^2), scaling is observed, and it is therefore assumed that the structure function is sensitive to the quark structure of the target. This scaling is a necessary, but not sufficient, condition of the Bjorken limit. However, the success of the scaling is taken as a strong indication that we are directly sensitive to the parton distributions. In addition, the quantitative observation of scaling is sufficient to make some connection between the structure function measured at finite Q^2 and in the Bjorken limit. If scaling is perfect, than the finite Q^2 structure function is equal to the high Q^2 structure function, even if one cannot explicitly show that the scattering is simply from quasifree quarks at lower Q^2 values. If the scaling is not perfect at low Q^2, the connection to the high-Q^2 structure can be made as long as the scaling violations are small enough or well understood.

Quantitative measurements of the deviation from scaling can be used to determine how precisely the data will match the value that would be measured in the scaling region. Thus, if these deviations are small enough, the structure functions measured at larger x values will be useful in constraining that large-x structure functions for the proton and for light nuclei. In addition, if they are target-independent, then any scaling violations will cancel in the EMC ratios, allowing us to extract these ratios at values of x larger than possible if one requires $W^2 > 4$ GeV^2. E89-008 took data on iron and deuterium at $Q^2 \approx 4$ GeV^2, but for $W^2 \lesssim 3$ GeV^2 [29]. Figure 11 shows the ratio of F_2^{Fe} to F_2^D for $1.3 < W^2 < 3.0$ GeV^2 (corrected for neutron excess in iron). Over this region, the data is in excellent agreement with previous measurements of the EMC effect. This test case indicates that scaling violations have little effect on the EMC ratio even for $W^2 < 2$GeV^2 at moderate Q^2. The situation should be even better for the larger Q^2 values of this measurement, which gives us confidence that the EMC effect measurements can be extended to larger x values (up to $x = 0.75$ if we require $W^2 > 3$ GeV^2, $x = 0.85$ for $W^2 > 2$ GeV^2).

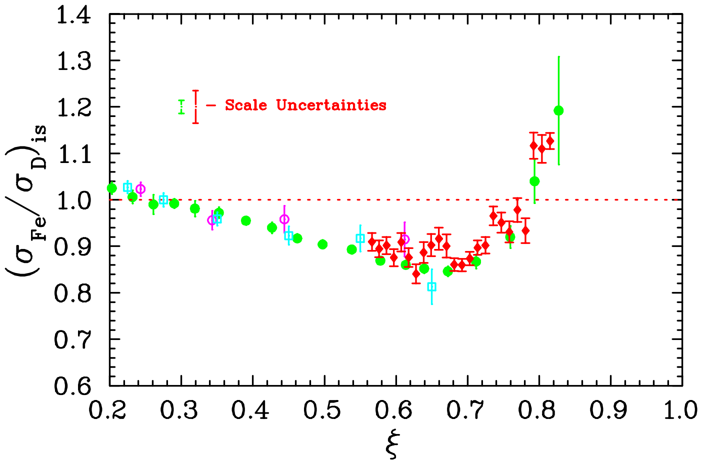

Figure 11: EMC ratio (Fe/D) for resonance region data from E89-008 (red diamonds) compared to world data. The JLab data are at $Q^2 \approx 4$ GeV^2, and cover a range in W^2 from 1.3 to 3.0 GeV^2. The error bars in the upper left indicate the size of the normalization uncertainty for the SLAC (green) and JLab (red) points.

One way to interpret the success of ξ-scaling in the resonance region is local duality. In 1970, Bloom and Gilman observed [31, 32] that the electroproduction of resonances in inclusive e-p scattering was closely related to the scaling limit in DIS scattering. Recent measurements at Jefferson Lab [33, 34] have examined duality in the proton more carefully, in both the separated and unseparated structure functions. Figure 12 shows the JLab data (plus two SLAC data sets at higher Q^2) along with a global fit to the data. For each fixed Q^2 data set, the resonance region structure function agrees with the fit globally (when averaged over the entire resonance region) and locally when averaged over any prominent resonance. The duality is observed at better than 10% for Q^2 values as low as 0.5 GeV^2. More recent measurements [35] have extended these measurements to show that duality holds in both longitudinal and transverse structure functions, and precision data will soon be available for similar studies for the polarized structure functions of the proton and neutron.

In a nucleus, the Fermi motion of the nucleons averages over the resonances, and so

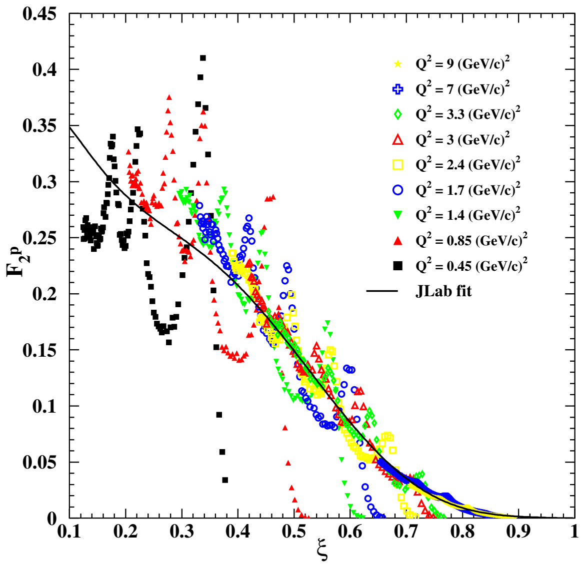

Figure 12: Hall C measurements of the resonance region structure function at low Q^2, and a fit to the combined data set.

rather than seeing *local* agreement between the DIS and resonance data, we see scaling at *all* values of ξ. Figure 13 shows how local duality in the proton structure function evolves into true scaling in ξ as the increasing Fermi motion of the nucleons washes out the resonance structure visible in the proton. In recent years, several efforts have begun to look into the theoretical basis for local duality. With a better understanding of the underlying cause of the observed duality, it may be possible to make a rigorous statement on the precision of ξ-scaling in nuclei. In the meantime, we can use the precision measurements of duality in the proton, along with our quantitative measurements of ξ-scaling in nuclei, to set an upper limit on possible scaling violations as we move from the DIS region into the resonance region. These measurements will help to determine how far in ξ we can extend these measurements while still maintaining the quantitative connection to the quark distributions of the nucleus.

4 EXPERIMENTAL REQUIREMENTS

We propose a measurement of inclusive electron scattering from hydrogen and light nuclei. Scattered electrons will be measured in the HMS and SOS spectrometers, which will run independently. The majority of the data will be taken in the HMS, while the SOS will be used to make measurements of electrons from background (charge symmetric) processes and to take additional data at the largest Q^2 values. All data will be taken at the highest

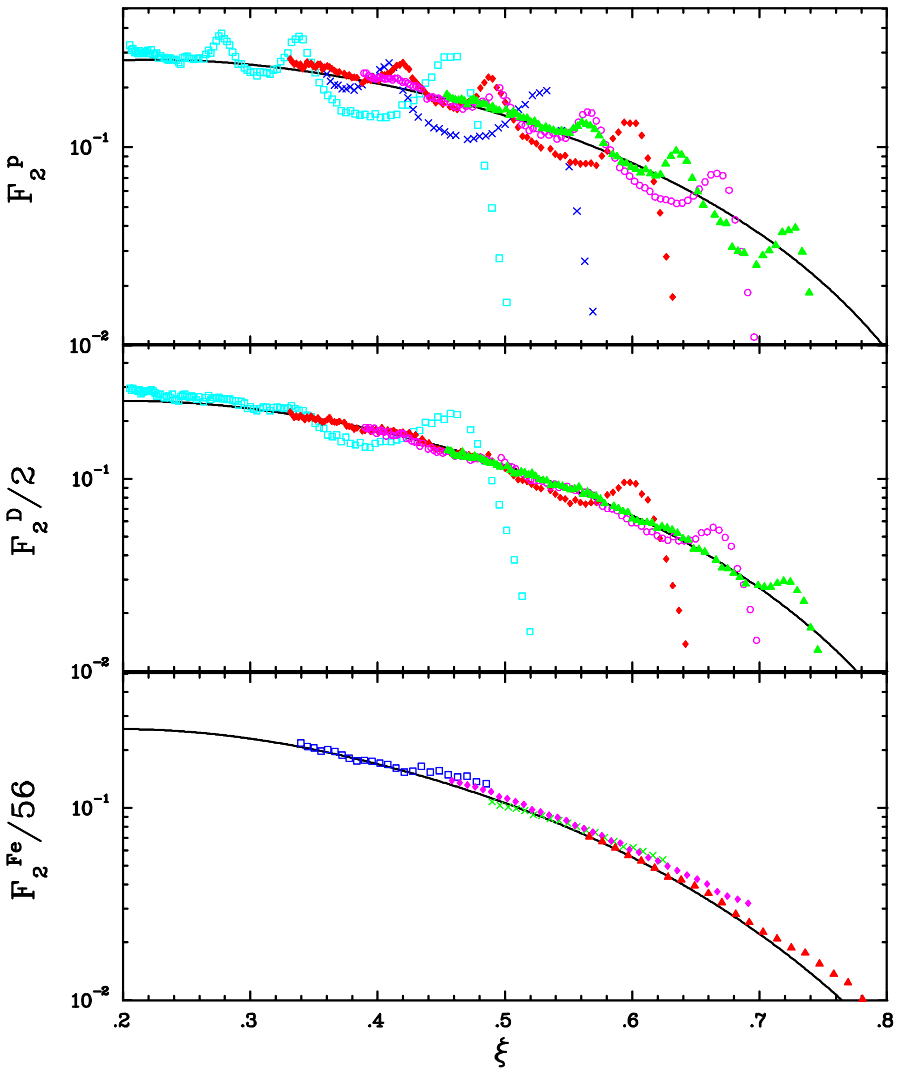

Figure 13: Resonance region structure functions for hydrogen, deuterium, and iron. For hydrogen, the elastic peak is excluded, for deuterium the quasielastic peak is subtracted from the data, and for iron there is a cut ($W^2 > 1.3$) to exclude the quasielastic contributions.

θ (deg)	E' (GeV)	x	Q^2 (GeV^2)	W^2 (GeV^2)	time (hours)
15	3.0-5.0 (4 settings)	0.26-1.0	1.2-2.0	0.9-5.4	22
23	2.1-4.0 (5 settings)	0.27-1.0	2.0-3.8	0.9-6.2	28
30	1.5-3.2 (6 settings)	0.29-1.0	2.4-5.2	0.9-6.9	33
45	0.75-2.1 (8 settings)	0.27-1.0	2.6-7.3	0.9-8.0	44
60	0.51-1.4 (10 settings)	0.24-1.0	2.5-8.6	0.9-9.0	99 52 †

† Additional time for running on solid targets.

Table 2: Kinematics for the proposed measurements. All data will be taken at 6 GeV beam energy. The run time includes time for all four targets, plus dummy running and overhead for target and momentum changes. In addition to the data on light nuclei, data will be taken on carbon, copper, and gold at the largest Q^2 setting.

beam energy available (6 GeV assumed for the proposed kinematics). We will take data at 5 angles, over a range of scattered electron energies covering $0.3 < x < 1.0$. Data will be taken on hydrogen, deuterium, ^{3}He, ^{4}He, and aluminum (for subtraction of the target endcap contributions). In addition, data will be taken on solid targets (C, Cu, and Au) at the highest Q^2 setting. This measurement uses the standard Hall C spectrometers and detector packages. The hydrogen and deuterium cryotargets are standard Hall C equipment, and we assume that the ^{3}He and ^{4}He targets will be able to run at beam currents of at least 40 μA, as was done on the previous Helium targets used for the 1999 kaon measurements.

Table 2 lists the kinematics we propose to measure, corresponding to the kinematics shown in Fig. 6. Target and momentum changes are included in the total time at each scattering angle. In all cases, data will be obtained utilizing 4 cm hydrogen, deuterium, ^{3}He, and ^{4}He cryogenic targets and a 3% (radiation length) aluminum target. We will run at currents between 20 and 50 μA with 6 GeV beam energy. Table 3 is a summary of the beam time required for the measurement. In addition to the data acquisition time, we have allocated time for checkout and background measurements, spectrometer angle changes, and one changeover from hydrogen and deuterium targets to helium targets.

One of the possible backgrounds for the measurement is electrons coming from charge symmetric processes such as the decay of neutral pions or pair production. We will make

Activity	Time (hours)
Production Running	226
Solid target running	52
Target Boiling Studies	12
Angle Changes (10)	10
Target Changeover	24
e^+ measurements	16
BCM calibrations	8
Beam spot monitoring	4
checkout/calibration	24
Total	376 (16 days)

Table 3: Beam time request for the proposed experiment. The time shown is for HMS running. The SOS will be used for more extensive measurements of the pion and charge symmetric backgrounds at lower momenta, where they are most likely to be a non-negligible contribution. The SOS will also be used for parasitic data taking at larger angles (Q^2), if the backgrounds are tolerable at these kinematics.

measurements of positrons in order to subtract the charge symmetric background. JLab experiment E89-008 was run at 4 GeV over a similar range of angles. For a scattering angle of 55°, they saw a maximum e^+/e^- ratio of 15%. However, this was for $x > 1$ and a thick target. At lower x values, the e^+/e^- ratio was typically at or below 10% for the thick target. For a thin target (similar in thickness to the targets we propose to use) the e^+/e^- ratio at larger angles (74°) was $\sim$ 20%. SLAC experiment E139 ran at higher energies (8-25 GeV) and found that the charge symmetric background was negligible for most of their kinematics, and largest ($\sim$10% on deuterium) at their lowest x and Q^2 values ($x < 0.1$). We do not expect large backgrounds except possibly at the lowest electron momentum settings and largest angle. Data will be taken in the SOS to determine the charge-symmetric backgrounds at these kinematics.

Pions are the other main source of background for the measurement. For the E89-008 experiment, the combination of the lead glass shower counter and the gas Čerenkov detector in the HMS (and SOS) provides pion rejection at $\sim$15,000:1 for a pion momentum of 1.0 GeV/c, and almost 100,000:1 for momenta above 1.5 GeV/c. For the high momentum settings, this is more than adequate to remove any pion contamination from the measurement. For lower momenta, the pion contamination may become non-negligible. Since E89-008, the calorimeter has been modified so that the front two layers are read out from both ends, so we expect the pion rejection for the low momentum pions to be better than the estimates above. We will have direct measurements of the pion backgrounds and

Source	Absolute Uncertainty	Relative Uncertainty	$\delta\sigma/\sigma(\%)$	$\delta R/R(\%)$ point-to-point	$\delta R/R(\%)$ scale	$\delta R/R$ (%) Statistical
HMS Momentum	<0.1%	0.01%	0.2	-	-	
Beam Energy	<0.1%	<0.02%	0.2	0.1	-	
θ	0.5mr	0.2mr	0.1	0.1	0.1	
t_D	0.5%		0.5	-	0.5	
t_{He}	1.0%		1.0	-	1.0	
Charge	0.4%	0.3%	0.5	0.42	0.2	
Target Boiling	<1.0%	0.5%	<1.0	0.3	0.3	
Endcap Subtraction	<1.0%	0.2%	<1.0	0.1	0.1	
Acceptance	1.0-2.0%	0.2%	1.0-2.0	0.2	-	
Radiative Corrections	2.0%	0.5%	2.0	0.3	0.4	
Detector Efficiency	0.5%	0.2%	0.5	0.2	-	
Deadtime Correction	<0.5%	0.2%	<0.5	0.1	0.2	
Total			2.7-3.3	0.7%	1.3	0.5-0.7
E139			3.3-3.7	1.6%	2.2	1.0-2.2

Table 4: Systematic uncertainties in the ratio $\sigma_{He}/\sigma_{^2H}$, compared to E139 uncertainties (for ^{4}He).

can make a correction for pion contamination if there are kinematics where there is some small contamination left after the PID cuts.

We estimate a systematic uncertainty of 3-4% in the measured cross sections for most of the kinematics. To correct for density changes due to localized heating in the cryotargets, we will measure rate as a function of current for each target. As this effect depends on the intrinsic beam spot size in addition to the raster size, we will make regular checks of the beam size, to insure that it does not vary significantly. Many sources of uncertainty will cancel in the cross section ratios for different targets, and we estimate a final systematic uncertainty in the ratios of ~1.6%. Table 4 shows the contributions to the systematic uncertainties in the target ratios. The solid targets will be measured at the same time as the deuterium targets, and so will not have uncertainties in the EMC ratios due to uncertainties in the kinematics (or target boiling effects). However, they will have larger uncertainties in the acceptance, due to the difference in the target length. The final uncertainty in the EMC ratio for solid targets and helium targets will be nearly identical. Note that the uncertainty in the thickness of the deuterium target is a common uncertainty for the $\sigma_A/\sigma_{^2H}$ ratios for all targets. Figures 14 and 15 show the projected uncertainties for the ^{3}He and ^{4}He EMC ratios.

5 SUMMARY

We request 16 days in Hall C to measure inclusive scattering for hydrogen, deuterium, ^{3}He, and ^{4}He for x>0.3 and $Q^2 \geq 1.0$ GeV^2. At the highest Q^2 value, we will take data

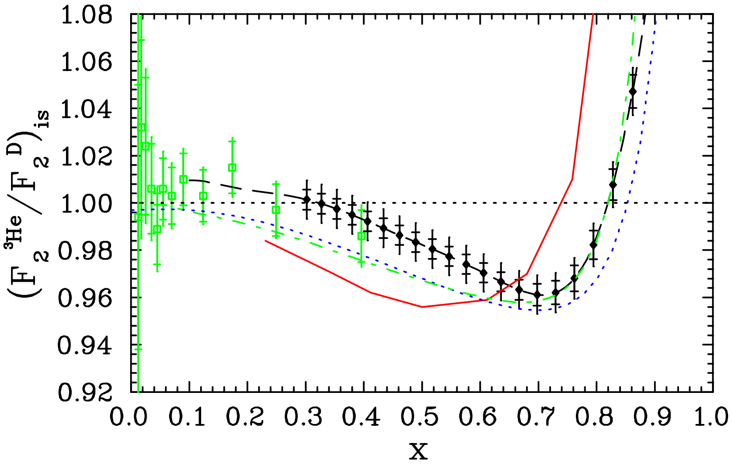

Figure 14: Projected uncertainties for the ^{3}He EMC ratios, along with the existing HERMES data. The inner error bars are statistical, while the outer error bars are statistical and point-to-point systematic errors. An overall normalization uncertainty of 1.3% is not shown. The dashed line is the fit to heavy nuclei, scaled to ^{3}He, while the solid red line is the calculation of Benhar *et al.* [15], and the dotted line is the calculation of Smirnov *et al.* [14].

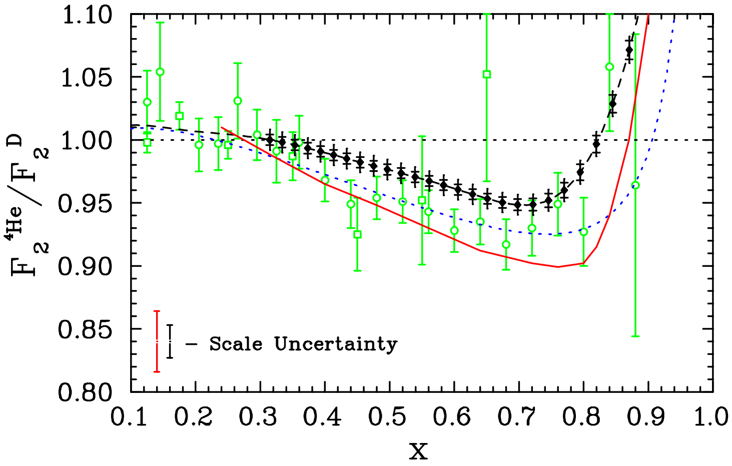

Figure 15: Projected uncertainties for the ^{4}He EMC ratios, along with the world data (mostly from SLAC E139 at large x). The inner error bars are statistical, while the outer error bars are statistical and point-to-point systematic errors. The overall normalization uncertainty of 1.3% is shown, as well as the SLAC normalization uncertainty. The curves are the same as in Fig. 14

at lower x values to determine where the nuclear effects go to zero (the crossover point from the anti-shadowing regime to the EMC effect regime). We will significantly improve the measurement of $\sigma_A/\sigma_{^2H}$ in ^{4}He and make the first measurement for the structure function and the EMC effect for ^{3}He over this x range. Both the A-dependence and the x-dependence of the EMC effect in these very light nuclei are unknown, and will constrain models of the EMC effect. At the highest Q^2, we will also take data on heavy targets. This will provide a single data set with the EMC ratios over a large range in A, as well as constraining the high-x behavior of the EMC effect if precise scaling extends to these x and Q^2 values, as indicated by the data from E89-008.

References

[1] J.J. Aubert *et al.*, Phys. Lett. **123B**, 275 (1983)

[2] Benvenuti *et al.*, Phys. Lett. B **189** 483 (1987)

[3] J. Gomez *et al.*, Phys. Rev. D **49** 4348 (1994)

[4] D. F. Geesaman, K. Saito and A.W. Thomas, Annu. Rev. Nucl. Part. Sci. **45** 337 (1995)

[5] A. Bodek and J.L. Ritchie, Phys. Rev. D **23**, 1070 (1981); **24**, 1400 (1981)

[6] S.V. Akulinichev *et al.*, Phys. Lett. B **158**, 485 (1985); Phys. Rev. Lett. **55**, 2239 (1985)

[7] C. Ciofi degli Atti and S. Liuti, Phys. Lett. B **225** 215 (1989); Phys. Rev. C **41**, 1100 (1990)

[8] D.M. Alde *et al.*, Phys. Rev. Lett. **64** 2479 (1990)

[9] Phys. Rev. C **65**, 055206 (2002)

[10] L.L. Frankfurt and M.I. Strikman, Phys. Rep. **160**, 235 (1988)

[11] J.P. Chen *et al.*, Phys. Rev. Lett. **66**, 1283 (1991)

[12] J. Arrington *et al.*, in preparation.

[13] C.W. DeJager, H. De Vries and C. De Vries, At. Data Nucl. Data Tables **14**, 479 (1974)

[14] G.I. Smirnov, Eur. Phys. J. C **10**, 239 (1999); V.V. Burov, A.V. Molochkov, and G.I. Smirnov, Preprint arXiv:nucl-th/9904050, Apr. 1999.

[15] O. Benhar, private communication.

[16] I. R. Afnan *et al.*, JLab Theory Note JLAB-THY-03-30, Submitted to Phys. Rev. C

[17] K. Ackerstaff *et al.*, Phys. Lett. B **475**, 386 (2000)

[18] J.J. Aubert *et al.*, Nucl. Phys. B **293**, 740 (1987)

[19] Allasia *et al.*, Zeit. Phys. C **28**, 321 (1991)

[20] G.R. Farrar and D.R. Jasckson, Phys. Rev. Lett. **35**, 1416 (1975)

[21] S.J. Brodsky, M. Burkardt and I. Schmidt, Nucl. Phys. B **441** 197 (1995)

[22] A. Bodek *et al.*, Phys. Rev. D **20**, 1471 (1979)

[23] L. W. Whitlow, S. Rock, A. Bodek, E. M. Riordan, and S. Dasu, Phys. Lett. **B250**, 193 (1990)

[24] W. Melnitchouk and A.W. Thomas, Phys. Lett. B **377**, 11 (1996)

[25] H. Fenker, C. Keppel, S. Kuhn, W. Malnitchouk, JLab experiment E03-012

[26] I. R. Afnan *et al.*, Phys. Lett. B **493**, 36 (2000)

[27] H. Georgi and H. D. Politzer, Phys. Rev. D 14, 1829 (1976).

[28] B. W. Filippone *et al.*, Phys. Rev. C **45**, 1582 (1992)

[29] J. Arrington, Ph.D. Thesis, Caltech (1998); J. Arrington *et al.*, Phys. Rev. C **64**, 014602 (2001)

[30] L.W. Whitlow *et al.*, Phys. Lett. B **282**, 475 (1992)

[31] E.D. Bloom and F.J. Gilman, Phys. Rev. D **4**, 2901 (1970)

[32] E.D. Bloom and F.J. Gilman, Phys. Rev. Lett. **25**, 1140 (1970)

[33] I. Niculescu *et al.*, Phys. Rev. Lett. **85**, 1186 (2000)

[34] R. Ent *et al.*, Phys. Rev. D **62**, 073008 (2000)

[35] CEBAF Experiment E94-110, C. Keppel, spokesperson.